



High-rate and ultra-stable Na-ion storage for Ni_3S_2 nanoarrays via self-adaptive pseudocapacitance

Jun Tang ^a, Shibing Ni ^{a,b,c,*}, Dongliang Chao ^b, Jilei Liu ^b, Xuelin Yang ^{a,**}, Jinbao Zhao ^c

^a College of Materials and Chemical Engineering, Hubei Provincial Collaborative Innovation Center for New Energy Microgrid, Key Laboratory of Inorganic Nonmetallic Crystalline and Energy Conversion Materials, China Three Gorges University, Yichang, 443002, PR China

^b School of Physical and Mathematical Sciences, Nanyang Technological University, 637371, Singapore

^c State Key Laboratory of Physical Chemistry of Solid Surfaces, Xiamen University, Xiamen 361005, PR China



ARTICLE INFO

Article history:

Received 3 November 2017

Received in revised form

27 December 2017

Accepted 29 January 2018

Available online 31 January 2018

Keywords:

Self-adaptive

Pseudocapacitance

Nickel sulphide

Nanoarray

Sodium ion battery

ABSTRACT

Ni_3S_2 nanoarrays directly growing on Ni foam are fabricated via an electrochemical corrosion method and used as freestanding electrode for sodium ion batteries. Based on high electronic conductivity facilitated by the 3D Ni backbone and fast surface redox reactions rendered by the ultrathin thickness of the Ni_3S_2 nanoarrays, high pseudocapacitive contribution for the charge storage is induced in the Ni_3S_2 -Ni electrode. Remarkably, the capacitive contribution is self-adaptively enhanced in cycling owing to the gradually reduced and stabilized charge transfer resistance, triggering exceptional electrochemical performance. The Ni_3S_2 -Ni electrode delivers ultra-stable cycling with charge/discharge capacities of 344.2/350.6 mAh g⁻¹ after 200 cycles at 150 mA g⁻¹ as well as high capacity recovery of 427 mAh g⁻¹ after 70 cycles from 150 to 3000 mA g⁻¹. Meanwhile, practical application for the Ni_3S_2 -Ni electrode is also preliminarily assessed. It exhibits promising fast discharge/slow charge (750/150 mA g⁻¹) performance with initial discharge/charge capacities of 285.4/275.7 mAh g⁻¹ and 244.8/242.2 mAh g⁻¹ after 300 cycles. When matching with $\text{Na}_3\text{V}_2(\text{PO}_4)_3$ cathode, it delivers discharge capacity of 347.8 mAh g⁻¹ after 180 cycles at 200 mA g⁻¹.

© 2018 Elsevier Ltd. All rights reserved.

1. Introduction

Increasing demand for sustainable and clean energy sources has been intensively stimulated owing to the exhaustion of traditional nonrenewable fossil fuel and serious environment pollution during the past few decades. Both energy harvesting from nature, and storing via batteries and supercapacitor technologies are the center of current research worldwide. Li-ion batteries (LIBs) have become a favorable power source for portable electronics and electric/hybrid electric vehicle (EV/HEV) because of their long cycle life, low cost and high safety [1–3]. While the present LIBs technologies are quite mature, sodium-ion batteries (SIBs) caught up from behind are now receiving increasing attention partly due to the wide availability of Na sources and thus potentially low cost [4–10].

Three categories of anode materials for SIBs can also be distinguished as insertion, alloying and conversion type, respectively, according to the charge/discharge mechanisms which is similar to that for LIBs. While insertion type anode materials perform poorly because of bigger size and sluggish kinetics of Na ions, and alloying type anode materials suffer from severe volume expansion [11–14], conversion anode materials have come into the spotlight for research owing to the moderate reaction kinetics and volume variation [15–19]. Typically, Ni_3S_2 has got attention owing to its low room temperature resistivity of $\sim 1.2 \times 10^{-4} \Omega \text{ cm}$ [20,21], much lower than its oxide counterparts, demonstrating great potential as anode for SIBs [21–24]. For instance, Qin et al. fabricated layered Ni_3S_2 -RGO via microwave assisted route and subsequent sintering, which shows reversible capacity of 391.6 mAh g⁻¹ after 50 cycles at 100 mA g⁻¹ [22]. Shang et al. prepared PEDOT decorated Ni_3S_2 , which shows reversible capacity of 280 mAh g⁻¹ after 30 cycles [23]. Despite high reversible capacity achieved up to now, challenges for Ni_3S_2 SIB electrode are still there, such as i) poor rate capability and unsatisfactory cycling performance, and ii) the practical feasibility of NiS in full cell is unexplored.

Capacitive charge storage has been demonstrated effective to

* Corresponding author. College of Materials and Chemical Engineering, Hubei Provincial Collaborative Innovation Center for New Energy Microgrid, Key Laboratory of Inorganic Nonmetallic Crystalline and Energy Conversion Materials, China Three Gorges University, Yichang, 443002, PR China.

** Corresponding author.

E-mail addresses: shibingni07@126.com (S. Ni), xlyang@ctgu.edu.cn (X. Yang).

prompt fast reaction kinetics in conventional Na-ion battery materials (insertion, conversion and alloying type), compared with the diffusion-controlled process [25–27]. In particular, extrinsic pseudocapacitance correlating with surface or near-surface redox reactions would be triggered when electrode materials are made into nanoscale dimensions to maximize reaction sites, resulting in superior performance. For instance, ultrathin nanoarrays of SnS and SnS₂ directly growing on electric graphene foam and TiO₂ nanosheet arrays growing on both sides of graphene sheets exhibit exceptional rate capability as anode for Na-ion batteries [28–30].

Here in this paper, we demonstrate for the first time, triggering superior sodium storage in Ni₃S₂ nanosheet arrays in-situ growing on Ni foam, through an extrinsic pseudocapacitive contribution. High reaction kinetics were boosted in the Ni₃S₂-Ni architecture, with 3D interconnected Ni backbone providing high efficient passway for electron transfer, and hierarchical pores (microsized pores in Ni backbone and nanosized pores in Ni₃S₂ nanoarrays) facilitating the contact between electrolyte and active Ni₃S₂ (schematic formation and morphology merits see Fig. 1). Furthermore, the ultrathin thickness of Ni₃S₂ nanosheets (less than 10 nm) renders fast surface or near-surface redox reactions, triggering high pseudocapacitive contribution to sodium ion storage. Remarkably, the charge transfer resistance of the Ni₃S₂-Ni electrode decreases along with cycle number and gradually reach stable, which facilitates the reaction kinetics for capacitive charge storage in cycling. As a result, the Ni₃S₂-Ni electrode exhibits exceptional electrochemical performance: 1) high stability with initial discharge/charge capacities of 496.3/445.3 mAh g⁻¹, maintaining of 350.6/344.2 mAh g⁻¹ after 200 cycles; 2) prominent rate capability with capacity recovery of 427 mAh g⁻¹ after 70 cycles from 150 to 3000 mA g⁻¹; 3) promising fast discharge/slow charge (750/150 mA g⁻¹) performance with discharge/charge capacities of 244.8/242.2 mAh g⁻¹ after 300 cycles. Besides, the full cell performance of the Ni₃S₂-Ni, matching with Na₃V₂(PO₄)₃ cathode, was also firstly evaluated in this manuscript, and the excellent performance (high discharge capacity of 347.8 mAh g⁻¹ after 180 cycles at 200 mA g⁻¹) indicates great potential for practical application.

2. Experimental section

2.1. Sample preparation

The chemicals were analytical grade and purchased from Shanghai Chemical Reagents. Ni foam (100 PPI pore size, 380 g m⁻² surface density, 1.5 mm thick) was purchased from Changsha Lyrun New Material corporation. In a typical procedure, 5 mmol thiourea were added in 20 ml distilled water. After stirring for 30 min, the transparent solution was transferred into a 50 ml teflonlined autoclave. Then Ni foams were placed in the autoclave, and distilled water was subsequently added to 80% of its capacity. The autoclave was at last sealed and placed in an oven, heated at 120 °C for 24 h. The mass of Ni foam before (m₁) and after sulfuration (m₂) was weighted by a microbalance. The weight of active Ni₃S₂ electrode is derived from m_{Ni₃S₂} = Δm × 240.21/64.12, where Δm = m₂ - m₁.

2.2. Composition, structure and morphology characterization

The composition, structure and morphology of the resulting products were characterized by X-Ray powder diffraction (Rigaku Ultima IV Cu Kα radiation $\lambda = 1.5406 \text{ \AA}$), X-Ray photoelectron spectroscopy (XPS, Thermo Fisher, K-Alpha 1063), field-emission scanning electron microscopy (FESEM, Model JSM-7600F, JEOL Ltd., Tokyo, Japan) and transmission electron microscopy (TEM, FEI, Tecnai G2 F30) equipped with selected area electron diffraction (SAED).

2.3. Electrochemical characterization

For preparing anode, the as-prepared Ni₃S₂-Ni discs (diameter of 14 mm) were dried at 120 °C for 12 h in a vacuum oven. Half cells (2025 coin-type) were assembled in an argon-filled dry box (MIKROUNA, Super 1220/750, H₂O < 1.0 ppm, O₂ < 1.0 ppm). The electrolyte is 1 M NaPF₆ in ethylene carbonate, dimethyl carbonate and diethyl carbonate (EC/DMC/DEC, 1:1:1 v/v/v) with 5% FEC additives and the separator membrane is Grade GF/D (Whatman). For the

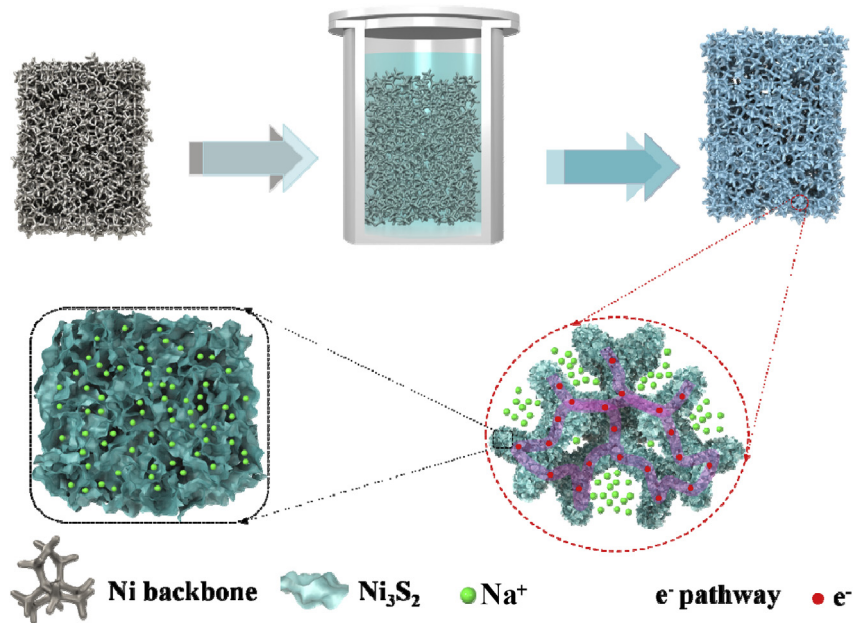


Fig. 1. The schematic illustration for the formation and morphology merits of the Ni₃S₂-Ni.

fabrication of $\text{Na}_3\text{V}_2(\text{PO}_4)_3$ cathode, a mixture of $\text{Na}_3\text{V}_2(\text{PO}_4)_3$, acetylene black, and polyvinylidene fluoride (PVDF) dissolved in N-methylpyrrolidine (NMP) solution (0.02 g ml^{-1}) with weight ratio of 7.5:1.5:1 were coated on aluminium foil and cut into disc electrodes (diameter of 14 mm). Full cells (2025 coin-type) with the $\text{Na}_3\text{V}_2(\text{PO}_4)_3$ cathode and the Ni_3S_2 -Ni anode were assembled using the same technology of half cells. Considering the initial irreversible Na ions consumption in charging, a capacity ratio of 1.2:1 between cathode and anode in full cells was adopted. Galvanostatic charge/discharge tested in the range of 0.02–3 V for half cells and 1.5–3.0 V for full cells was used characterized on a multichannel battery test system (LAND CT2001A). The cyclic voltammetry (CV) measurement of the electrodes (vs. Na/Na^+) was measured on a CHI660C electrochemical workstation. Electrochemical impedance spectroscopy (EIS) measurements were performed on CHI660C electrochemical workstation under open circuit conditions over a frequency range from 100 kHz to 0.01 Hz by applying an AC signal of 5 mV in amplitude throughout the tests.

3. Results and discussion

XRD pattern of the as-prepared sample is shown in Fig. 2(a). As seen, the diffraction peaks located at 44.7° , 52.1° and 76.6° can be attributed to the Ni (111), (200) and (220) faces, respectively (JCPDS,

No. 87-0712). Others diffraction peaks which located at 21.9° , 31.3° , 38.0° , 44.7° , 50.1° , 55.0° , 55.6° and 69.4° can be indexed as the (010), (−110), (111), (020), (120), (−121), (−211) and (030) faces of rhombohedral Ni_3S_2 with lattice constants $a = b = c = 4.0718 \text{ \AA}$, which is in good agreement with JCPDS, No. 73-0698. The composition of the sample was further confirmed by XPS. As showed in Fig. 2(b), two main peaks at 873.2 and 855.7 eV can be assigned to $\text{Ni } 2p_{1/2}$ and $\text{Ni } 2p_{3/2}$, respectively. Two peaks near 861.3 and 852.6 eV can be ascribed to the satellite of $\text{Ni } 2p_{1/2}$, the peak at 879.7 eV can be ascribed to the satellite of $\text{Ni } 2p_{3/2}$ [5,6,21,31–34]. The high resolution spectrum of S 2p is shown in Fig. 2(c). As seen, two strong peaks near 163.3 and 162.1 eV can be assigned to $\text{S } 2p_{1/2}$ and $\text{S } 2p_{3/2}$, respectively [5,6,21,32,33]. The coarse morphology in Fig. 2(d) differs much from Ni foam (the inset), implying the growth of Ni_3S_2 on Ni. Fig. 2(e) suggests the Ni_3S_2 are of porous architecture, consisting of interwoven nanoflakes with lateral size $\sim 1 \mu\text{m}$. The formation of Ni_3S_2 nanoarrays stems from an electrochemical corrosion process, and detailed electrochemical reactions can be described as follows:

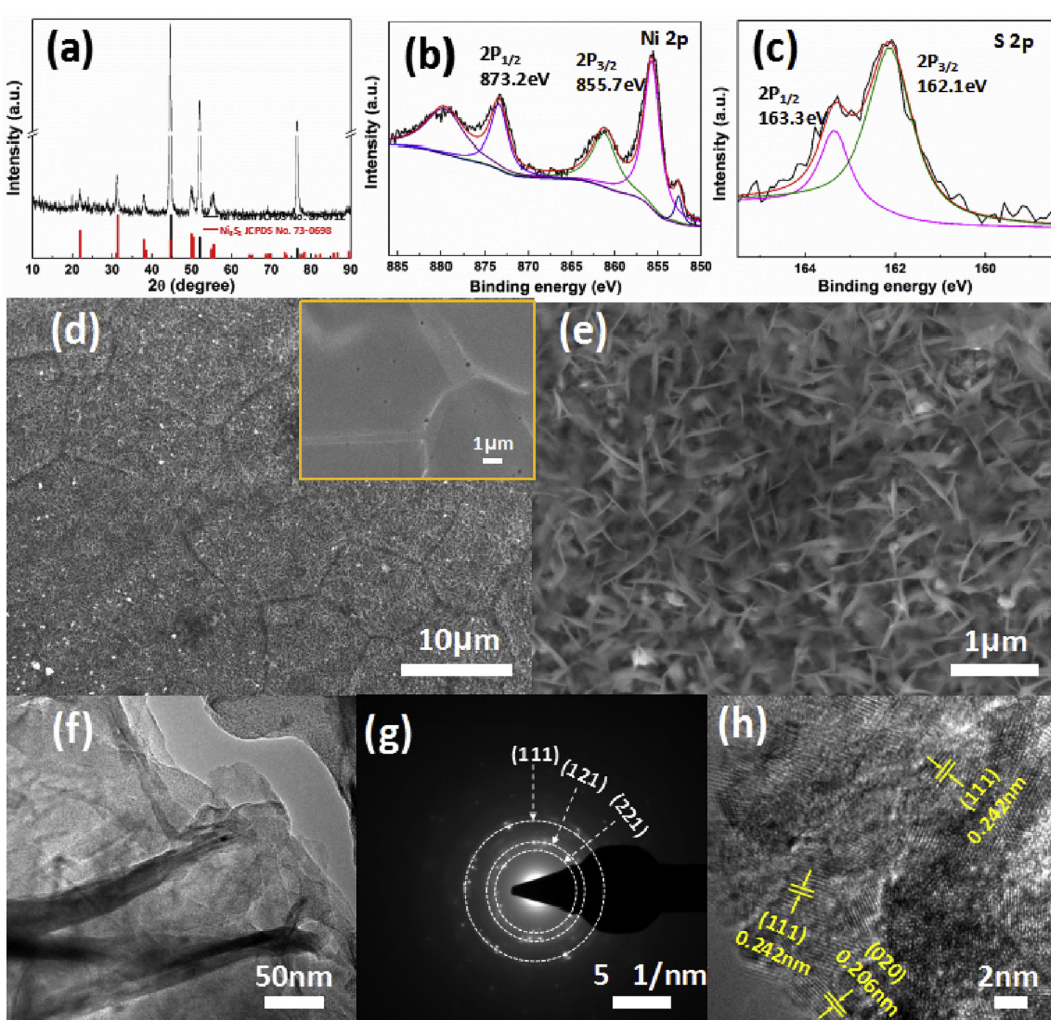
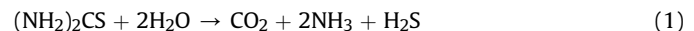
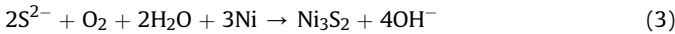


Fig. 2. (a) XRD pattern, high resolution XPS spectra of (b) Ni 2p and (c) S 2p, (d) low and (e) high magnification SEM images, (f) TEM, (g) SAED pattern and (h) HRTEM image of the Ni_3S_2 -Ni. The inset of (a) is a SEM image of Ni foam.



Such electrochemical corrosion process is similar to that of $Ni(OH)_2$ obtained under similar circumstance [35].

TEM image in Fig. 2(f) clearly exhibits the sheet-like morphology of the Ni_3S_2 , and the thickness of these nanosheets is less than 10 nm. Diffraction spots distributed as rings (Fig. 2(g)) reveals the polycrystalline characteristics of the Ni_3S_2 . HRTEM image (Fig. 2(h))

of the Ni_3S_2 exhibits lattice fringes with interplanar spacing of 0.206 nm and 0.242 nm, which can be assigned to the (020) and (111) face of rhombohedral Ni_3S_2 .

The sodium storage performance of the Ni_3S_2 -Ni was evaluated in half cell. Fig. 3(a) is the cyclic voltammetric (CV) curves of the initial three cycles at a scan rate of 0.2 mV s^{-1} between 0 and 3.0 V. As seen, the profiles of CV curves for the 2nd and 3rd are similar, whereas discrepancy between the 1st and subsequent two cycles

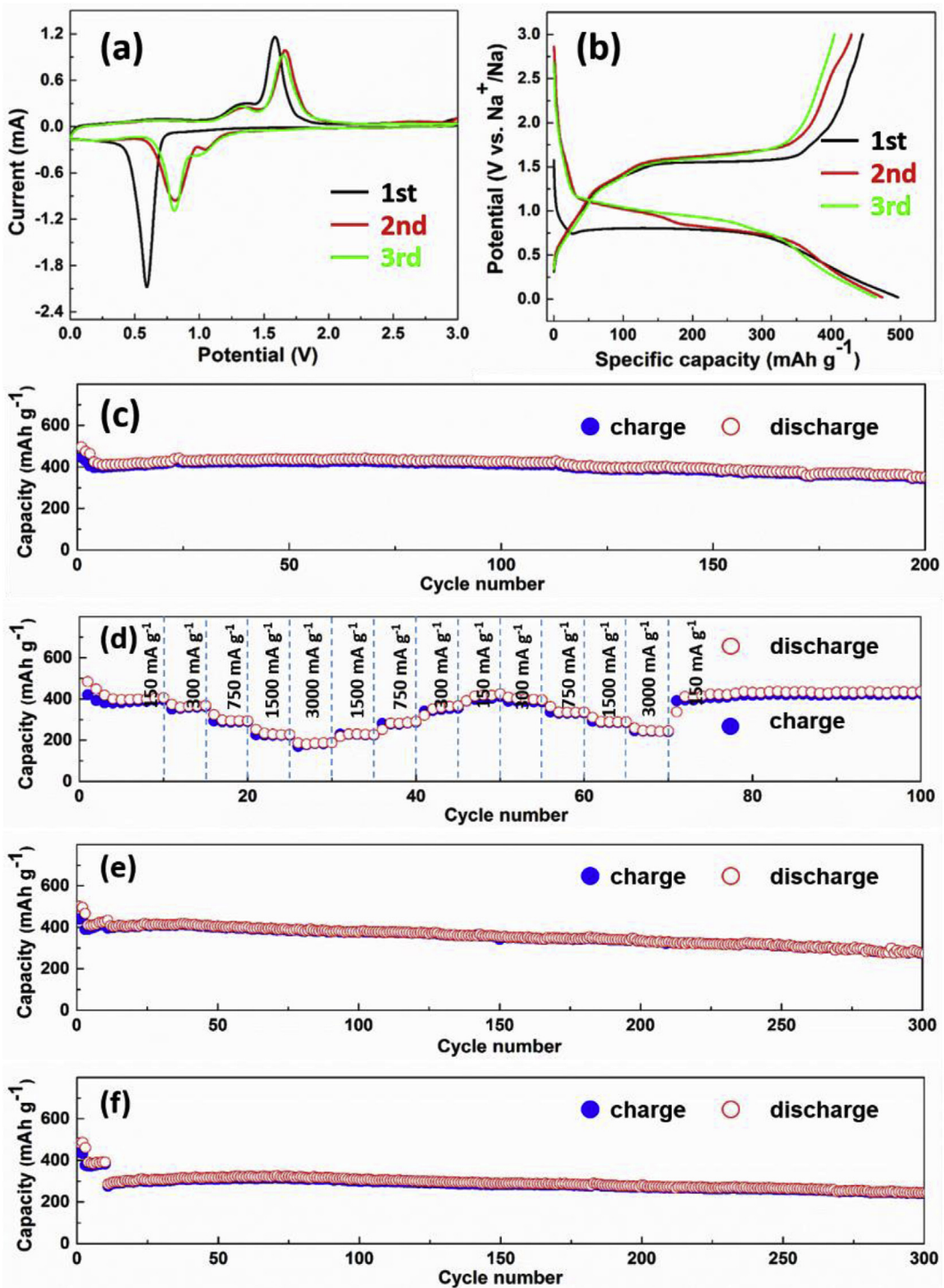


Fig. 3. Electrochemical performance of the Ni_3S_2 -Ni electrode. (a) Cyclic voltammograms at a scan rate of 0.2 mV s^{-1} . (b) Galvanostatic charge-discharge profiles and (c) Cycling performance at a specific current of 150 mA g^{-1} . (d) Rate performance, (e) Slow discharge/fast charge at $750/150\text{ mA g}^{-1}$. (f) Fast discharge/slow charge at $150/750\text{ mA g}^{-1}$.

Table 1

The summarization of charge capacity versus cycle number for various nickel sulphides electrodes for NIBs.

Electrode	Current mA g^{-1}	Charge capacity (mAh g^{-1})		Attenuation per lap (%)	Ref.
		/1st	/n		
NiS ₂ /GNS	100	~510	~305/200	0.20	[4]
NiS _x /CNT	100	410.9	300/130	0.21	[5]
NiS	100	590	499.9/50	0.30	[6]
Ni ₃ S ₂ /Ni	50	~330	~280/100	0.15	[21]
Ni ₃ S ₂ /RGO	100	~510	~400/50	0.35	[22]
Ni ₃ S ₂ /PEDOT	600	318.3	280/30	0.40	[23]
Ni ₃ S ₂	45	~440	~220/100	0.50	[24]
Ni ₃ S ₂ /Ni	150	445.3	344.2/200	0.11	this work

are displayed. In the 1st cathodic scan, a strong reduction peak near 0.61 V associates with the reduction of Ni₃S₂ to Ni and Na₂S ($\text{Ni}_3\text{S}_2 + 4\text{Na}^+ + 4\text{e}^- \rightarrow 2\text{Na}_2\text{S} + 3\text{Ni}$), as well as the formation of the solid electrolyte interface (SEI) [21–24]. It shifts to high voltage region and splits into two peaks near 0.76 and 1.0 V in subsequent cycles, owing to the activation of the electrode [22]. Two oxidation peaks near 1.34 V and 1.59 V can be observed in the 1st anodic scan, corresponding to the oxidation of Ni to Ni₃S₂ ($2\text{Na}_2\text{S} + 3\text{Ni} \rightarrow \text{Ni}_3\text{S}_2 + 4\text{Na}^+ + 4\text{e}^-$) [21–24]. After that, the oxidation peak near 1.59 V shifts to and stabilizes at 1.64 V, suggesting stable desodiation process. Fig. 3(b) is the initial three charge/discharge

curves. The potential regions are in accordance with the CV curves, and little variation of charge/discharge profiles suggests highly stable reaction process. As shown in Fig. 3(c), the Ni₃S₂-Ni exhibits initial discharge/charge capacities of 496.3/445.3 mAh g^{-1} , which attenuate slightly along with cycle number, maintaining of 350.6/344.2 mAh g^{-1} after 200 cycles. The electrochemical performance of the Ni₃S₂-Ni shows distinct improvement compared with reported nickel sulfides, as summarized in Table 1 [4–6,21–24]. Fig. 3(d) shows the rate performance of the Ni₃S₂-Ni electrode, which delivers charge capacity of 395.5, 362.5, 290.5, 223.7 and 188.5 mAh g^{-1} at the current densities of 150, 300, 750, 1500 and

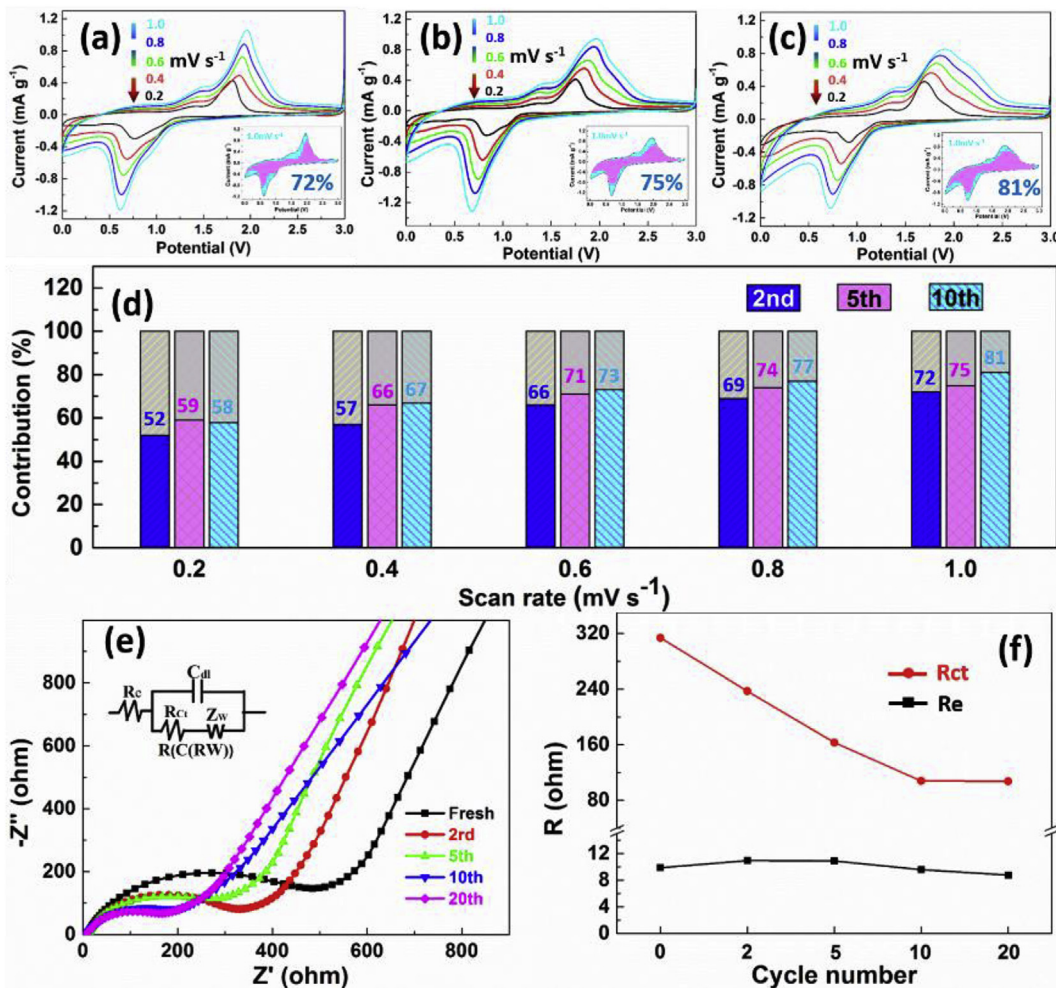


Fig. 4. CV curves of Ni₃S₂-Ni electrode at different scan rate after (a) 2, (b) 5 and (c) 10 cycles. (d) Pseudocapacitive contribution at different scan rates. (e) EIS spectra of the Ni₃S₂-Ni electrode and (f) corresponding values of R_{e} and R_{ct} with different states. The inset in (a), (b), (c) are capacitive contribution at a scan rate of 1 mV s^{-1} .

3000 mA g^{-1} , respectively. When reverting current density to 150 mA g^{-1} , high charge capacity of 427 mAh g^{-1} can be recovered. The capacity increasing in cycling stems from electrochemical activation that introduces extra sites for Na-ion storage, which is similar to that in MnO-Graphene, NiO-Ni, Cu_xO-Cu electrodes for LIBs [36–38]. The electricity consumption for electronic devices is usually irregular in daily life (i.e., a cell phone use for 2 days just needs charge 1–2 h). To simulate the practical situation, the Ni₃S₂-Ni anode was tested at irregular charge-discharge current. Fig. 3(e) shows the cycle performance of the Ni₃S₂-Ni at slow discharge (150 mA g^{-1}) and fast charge (750 mA g^{-1}), before which it was activated at 150 mA g^{-1} for 10 cycles. The discharge/charge capacities are $433.3/394.9 \text{ mAh g}^{-1}$ in the initial cycle and maintain of $274.3/273.7 \text{ mAh g}^{-1}$ after 300 cycles. Fast discharge (750 mA g^{-1}) and slow charge (150 mA g^{-1}) of the Ni₃S₂-Ni anode is also assessed for comparison. As seen, after 10 cycles activation at 150 mA g^{-1} , the discharge/charge capacities are $285.4/275.7 \text{ mAh g}^{-1}$ for the first cycle and retain $244.8/242.2 \text{ mAh g}^{-1}$ after 300 cycles. Close value of reversible capacities for the Ni₃S₂-Ni in different testing mode demonstrates great potential for practical application.

To understand the exceptional cycle stability and rate capability of the Ni₃S₂-Ni, the reaction kinetics of the electrode was studied. Fig. 4(a)–(c) are the CV curves of the Ni₃S₂-Ni electrode under different state from 0.2 to 1 mV s^{-1} , based on which the capacitance contribution in sodium storage can be deduced. According to equation of $i(V) = k_1 v + k_2 v^{1/2}$, the capacitive contribution to charge storage can be extracted by separating the $k_1 v$ part [28,30,39,40], where k_1 is constant can be determined by CV curves at different scan rate [30]. As expected, high pseudocapacitive contribution for the Ni₃S₂-Ni electrode was induced by the maximized reaction sites stemming from ultrathin nanoarray architecture of the Ni₃S₂. At a scan rate of 1 mV s^{-1} , capacitive contribution for the Ni₃S₂-Ni reach 72%, self-adaptively increasing to 75% and 81% after 5 and 10 cycles, respectively. Even at lower scan rate from 0.2 to 0.8 mV s^{-1} (Fig. 4(d)), capacitive contributions of the Ni₃S₂-Ni

electrode are always higher than 50%, demonstrating fast reaction kinetics. EIS spectra of the Ni₃S₂-Ni (Fig. 4(e)) were used to further elaborate the self-adaptive variation of the pseudocapacitive contribution. The intercept in high-frequency can be attributed to the SEI film and/or contact resistance (Re), the medium-frequency semicircle is due to the charge-transfer impedance on electrode/electrolyte interface (Rct), and the inclined line in low-frequency corresponds to the Na-ion diffusion process within the electrode [41,42]. According to an R (C (RW)) equivalent circuit fitting, it is found that Re shows little variation upon cycling, indicating stable contact between the electrode material and current collector. By contrast, Rct decreases gradually in 10 cycles and then maintains stable, suggesting enhanced charge transfer process in cycling. Based on the variation for Rct, the self-adaptive pseudocapacitive Na-ion storage for the Ni₃S₂-Ni electrode can be understood. The contact and diffusion of Na-ions with/within Ni₃S₂ are largely enhanced owing to the porous architecture and the ultrathin thickness of the Ni₃S₂ nanoarrays [28,30,43]. In contrast, the relative-low electron transmission may become a limitation for the fast electrochemical reactions. Once the electron transmission is enhanced, the whole charge storage will be spontaneously improved, resulting in self-adaptively pseudocapacitive contribution in cycling.

The Ni₃S₂-Ni was also demonstrated to be prospective in SIB full cell matching with Na₃V₂(PO₄)₃ (NVP) cathode. According to the typical charge/discharge curves of Ni₃S₂-Ni and NVP (Fig. 5(a)), voltage region of 3.0–1.5 V was selected for full cell testing. Similar profiles of the charge and discharge curves in Fig. 5(b) suggest stable electrochemical reactions in the whole cycling process. The cycle stability of a full cell is shown in Fig. 5(c). The capacity attenuates in the first few cycles and then gradually increases along with cycling number and reach stable, which may be relevant to the initial formation of SEI and the subsequent activation of the electrode [11,41]. After 180 cycles, it can still deliver high discharge capacity of 347.8 mAh g^{-1} , demonstrating great potential for

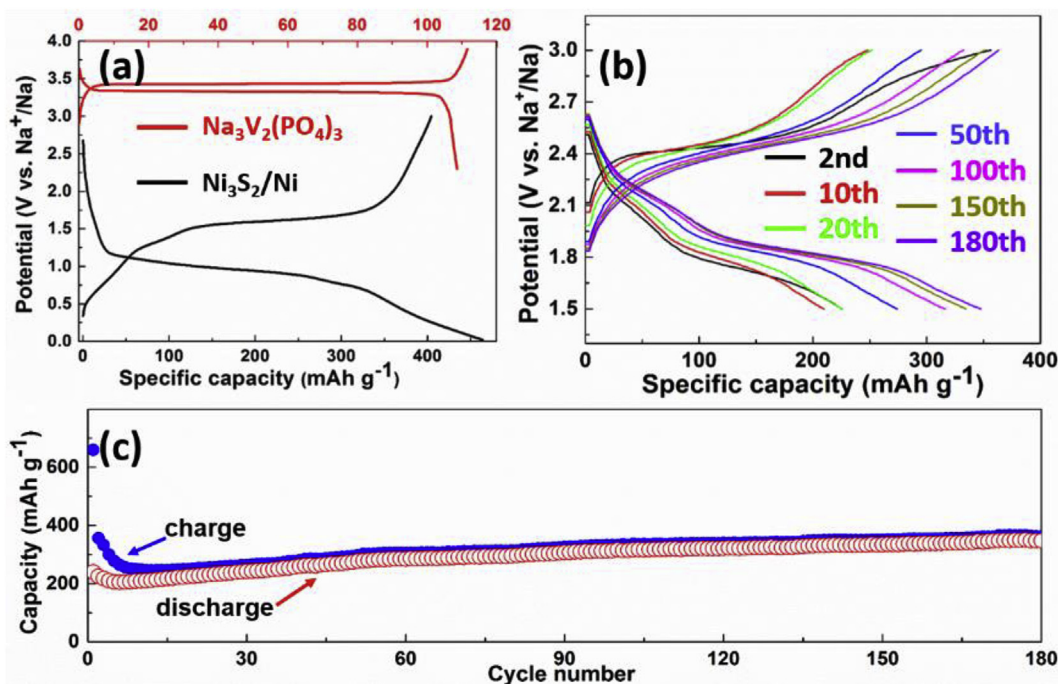


Fig. 5. Full cell performance of Ni₃S₂-Ni anode coupled with Na₃V₂(PO₄)₃ cathode. (a) Galvanostatic curves of the Ni₃S₂-Ni electrode and Na₃V₂(PO₄)₃ electrode in half cell. (b) Charge/discharge curves and (c) cycling performance of full cell at a specific current of 200 mA g^{-1} .

practical application.

4. Conclusions

In summary, ultrathin Ni₃S₂ nanoarrays directly growing on Ni foam was successfully prepared via an electrochemical corrosion method, which shows prominent electrochemical performance as freestanding anode for Na-ion batteries. It delivers high charge/discharge capacities of 344.2/350.6 mAh g⁻¹ after 200 cycles at 150 mA g⁻¹. After two periods (70 cycles) of rate capability testing from 150 to 3000 mA g⁻¹, high charge/discharge capacity of 427/436.4 mAh g⁻¹ can be recovered when reverting to 150 mA g⁻¹. The superior rate capability and the ultra-stable performance of the Ni₃S₂-Ni electrode are demonstrated to stem from high and self-adaptively pseudocapacitive contribution triggered by fast surface or near-surface reaction kinetics and enhanced electron transmission in cycling. Remarkably, when matching with the NVP cathode, the Ni₃S₂-Ni electrode also delivers prominent cycle stability with high reversible capacity of 347.8 mAh g⁻¹ after 180 cycles. These outstanding performances make our Ni₃S₂-Ni electrode be closer to practical application, and the inner mechanisms to boost the prominent performance of the Ni₃S₂ electrode may be referential for future research.

Acknowledgement

We gratefully acknowledge the financial support from Natural Science Foundation of China (NSFC 51672158, 51772169, 51572151) and the Outstanding Youth Science and Technology Innovation Team Project of Hubei Educational Committee (T201603).

References

- [1] H.L. Pan, Y.S. Hu, L.Q. Chen, Room-temperature stationary sodium-ion batteries for large-scale electric energy storage, *Energy Environ. Sci.* 6 (2013) 2338–2360.
- [2] D.P. Kundu, E. Talaie, V. Duffort, L.F. Nazar, The emerging chemistry of sodium ion batteries for electrochemical energy storage, *Angew. Chem. Int. Ed.* 54 (2015) 2–20.
- [3] D. Xie, X.H. Xia, W.J. Tang, Y. Zhong, Y.D. Wang, D.H. Wang, X.L. Wang, J.P. Tu, Novel carbon channels from loofah sponge for construction of metal sulfide/carbon composites with robust electrochemical energy storage, *J. Mater. Chem. A* 5 (2017) 7578–7585.
- [4] T.S. Wang, P. Hu, C.J. Zhang, H.P. Du, Z.H. Zhang, X.G. Wang, S.G. Chen, J.W. Xiong, G.L. Cui, Nickel disulfide-graphene nanosheets composites with improved electrochemical performance for sodium ion battery, *ACS Appl. Mater. Interfaces* 8 (2016) 7811–7817.
- [5] F.P. Zhao, Q.F. Gong, B. Traynor, D. Zhang, J.J. Li, H.L. Ye, F.J. Chen, N. Han, Y.Y. Wang, X.H. Sun, Y.G. Li, Stabilizing nickel sulfide nanoparticles with an ultrathin carbon layer for improved cycling performance in sodium ion batteries, *Nano Rev.* (2016) 3162–3170.
- [6] D. Zhang, W.P. Sun, Y. Zhang, Y.H. Dou, Y.Z. Jiang, S.X. Dou, Engineering hierarchical hollow nickel sulfide spheres for high-performance sodium storage, *Adv. Funct. Mater.* 26 (2016) 7479–7485.
- [7] D. Xie, W.J. Tang, Y.D. Wang, X.H. Xia, Y. Zhong, D. Zhou, D.H. Wang, X.L. Wang, J.P. Tu, Facile fabrication of integrated three-dimensional C-MoSe₂/reduced graphene oxide composite with enhanced performance for sodium storage, *Nano Rev.* 9 (2016) 1618–1629.
- [8] D. Xie, X.H. Xia, Y.D. Wang, D.H. Wang, Y. Zhong, W.J. Tang, X.L. Wang, J.P. Tu, Nitrogen-doped carbon embedded MoS₂ microspheres as advanced anodes for lithium- and sodium-ion batteries, *Chem. Eur. J.* 22 (2016) 11617–11623.
- [9] D. Xie, X.H. Xia, Y. Zhong, Y.D. Wang, D.H. Wang, X.L. Wang, J.P. Tu, Exploring advanced sandwiched arrays by vertical graphene and N-doped carbon for enhanced sodium storage, *Adv. Energy Mater.* 7 (2017), 1601804, 9p.
- [10] X. Li, J.H. Li, Q.S. Gao, X. Yu, R.Z. Hu, J. Liu, L.C. Yang, M. Zhu, MoS₂ nanosheets with conformal carbon coating as stable anode materials for sodium-ion batteries, *Electrochim. Acta* 254 (2017) 172–180.
- [11] Y.M. Li, S.Y. Xu, X.Y. Wu, J.Z. Yu, Y.S. Wang, Y.S. Hu, H. Li, L.Q. Chen, X.J. Huang, Amorphous monodispersed hard carbon micro-spherules derived from biomass as a high performance negative electrode material for sodium-ion batteries, *J. Mater. Chem. A* 3 (2015) 71–77.
- [12] L. Wu, H.Y. Lu, L.F. Xiao, X.P. Ai, H.X. Yang, Y.L. Cao, Electrochemical properties and morphological evolution of pitaya-like Sb@C microspheres as high-performance anode for sodium ion batteries, *J. Mater. Chem. A* 3 (2015) 5708–5713.
- [13] A. Kohandehghan, K. Cui, M. Kupsta, J. Ding, E.M. Lotfabad, W.P. Kalisvaart, D. Mitlin, Activation with Li enables facile sodium storage in germanium, *Nano Lett.* 14 (2014) 5873–5882.
- [14] X.Q. Xie, D.W. Su, K. Kretschmer, J.Q. Zhang, B. Sun, G.X. Wang, Sn@CNT nanopillars grown perpendicularly on carbon paper: a novel free-standing anode for sodium ion batteries, *Nano Energy* 13 (2015) 208–217.
- [15] X.D. Xu, W. Liu, Y. Kim, J. Cho, Nanostructured transition metal sulfides for lithium ion batteries: progress and challenges, *Nano Today* 9 (2014) 604–630.
- [16] S.Y. Li, B.H. Qu, H. Huang, P. Deng, C.H. Xu, Q.H. Li, T.H. Wang, Controlled synthesis of iron sulfide coated by carbon layer to improve lithium and sodium storage, *Electrochim. Acta* 247 (2017) 1080–1087.
- [17] M.H. Chen, J.W. Zhang, X.H. Xia, M.L. Qi, J.H. Yin, Q.G. Chen, Construction of cobalt sulfide/nickel core-branch arrays and their application as advanced electrodes for electrochemical energy storage, *Electrochim. Acta* 195 (2016) 184–191.
- [18] W. Qin, D.S. Li, X.J. Zhang, D. Yan, B.W. Hu, L.K. Pan, ZnS nanoparticles embedded in reduced graphene oxide as high performance anode material of sodium-ion batteries, *Electrochim. Acta* 191 (2016) 435–443.
- [19] X. Wang, J.F. Huang, J.Y. Lia, L.Y. Cao, W. Hao, Z.W. Xu, Q. Kang, Controlling the layered structure of WS₂ nanosheets to promote Na⁺ insertion with enhanced Na-ion storage performance, *Electrochim. Acta* 222 (2016) 1724–1732.
- [20] J. Wang, D.L. Chao, J.L. Liu, L.L. Li, L.F. Lai, J.Y. Lin, Z.X. Shen, Ni₃S₂@MoS₂ core/shell nanorod arrays on Ni foam for high-performance electrochemical energy storage, *Nano Energy* 7 (2014) 151–160.
- [21] X.S. Song, X.F. Li, Z.M. Bai, B. Yan, D.J. Li, X.L. Sun, Morphology-dependent performance of nanostructured Ni₃S₂/Ni anode electrodes for high performance sodium ion batteries, *Nano Energy* 26 (2016) 533–540.
- [22] W. Qin, T.Q. Chen, T. Lu, D.H.C. Chua, L.K. Pan, Layered nickel sulfide-reduced graphene oxide composites synthesized via microwave-assisted method as high performance anode materials of sodium-ion batteries, *J. Power Sources* 302 (2016) 202–209.
- [23] C.Q. Shang, S.M. Dong, S.L. Zhang, P. Hu, C.J. Zhang, G.L. Cui, A Ni₃S₂-PEDOT monolithic electrode for sodium batteries, *Electrochim. Commun.* 50 (2015) 24–27.
- [24] H.S. Ryu, J.S. Kim, J. Park, J.Y. Park, G.B. Cho, X.J. Liu, I.S. Ahn, K.W. Kim, J.H. Ahn, J.P. Ahn, S.W. Martin, G.X. Wang, H.J. Ahn, Degradation mechanism of room temperature Na/Ni₃S₂ cells using Ni₃S₂ electrodes prepared by mechanical alloying, *J. Power Sources* 244 (2013) 764–770.
- [25] H. Xiong, M.D. Slater, M. Balasubramanian, C.S. Johnson, T. Rajh, Amorphous TiO₂ nanotube anode for rechargeable sodium ion batteries, *J. Phys. Chem. Lett.* 2 (2011) 2560–2565.
- [26] Z. Hu, L.X. Wang, K. Zhang, J.B. Wang, F.Y. Cheng, Z.L. Tao, J. Chen, MoS₂ nanoflowers with expanded interlayers as high-performance anodes for sodium-ion batteries, *Angew. Chem.* 126 (2014) 13008–13012.
- [27] V. Augustyn, P. Simon, B. Dunn, Pseudocapacitive oxide materials for high-rate electrochemical energy storage, *Energy Environ. Sci.* 7 (2014) 1597–1614.
- [28] D.L. Chao, P. Liang, Z. Chen, L.Y. Bai, H. Shen, X.X. Liu, X.H. Xia, Y.L. Zhao, S.V. Savilov, J.Y. Lin, Z.X. Shen, Pseudocapacitive Na-ion storage boosts high rate and areal capacity of self-branched 2D layered metal chalcogenide nanoarrays, *ACS Nano* 10 (2016) 10211–10219.
- [29] C.J. Chen, Y.W. Wen, X.L. Hu, X.L. Ji, M.Y. Yan, L.Q. Mai, P. Hu, B. Shan, Y.H. Huang, Na⁺ intercalation pseudocapacitance in graphene-coupled titanium oxide enabling ultra-fast sodium storage and long-term cycling, *Nat. Commun.* 6 (2015), 6929, 8p.
- [30] D.L. Chao, C.R. Zhu, P.H. Yang, X.H. Xia, J.L. Liu, J. Wang, X.F. Fan, S.V. Savilov, J.Y. Lin, H.J. Fan, Z.X. Shen, Array of nanosheets render ultrafast and high-capacity Na-ion storage by tunable pseudocapacitance, *Nat. Commun.* 7 (2016), 12122, 8p.
- [31] Y.J. Ruan, D.C. Zha, L. Lv, B. Zhang, J. Liu, X. Ji, C.D. Wang, J.J. Jiang, Al-doped β-NiS mesoporous nanoflowers for hybrid-type electrodes toward enhanced electrochemical performance, *Electrochim. Acta* 236 (2017) 307–318.
- [32] V. Biju, Ni 2p X-ray photoelectron spectroscopy study of nanostructured nickel oxide, *Mater. Res. Bull.* 42 (2007) 791–796.
- [33] J.M. Falkowski, N.M. Concannon, B. Yan, Y. Surendranath, Heazlewoodite, Ni₃S₂: a potent catalyst for oxygen reduction to water under benign conditions, *J. Am. Chem. Soc.* 137 (2015) 7978–7981.
- [34] A. Galtayries, C. Cousi, S. Zanna, P. Marcus, SO₂ adsorption at room temperature on Ni (111) surface studied by XPS, *Surf. Interface Anal.* 36 (2004) 997–1000.
- [35] S.B. Ni, X.H. Lv, T. Li, X.L. Yang, L.L. Zhang, The investigation of Ni(OH)₂/Ni as anodes for high performance Li-ion batteries, *J. Mater. Chem. A* 1 (2013) 1544–1547.
- [36] Y.M. Sun, X.L. Hu, W. Luo, F.F. Xia, Y.H. Huang, Reconstruction of conformal nanoscale MnO on graphene as a high-capacity and long-life anode material for lithium ion batteries, *Adv. Funct. Mater.* 23 (2013) 2436–2444.
- [37] S.B. Ni, X.H. Lv, T. Li, X.L. Yang, L.L. Zhang, Y. Ren, A novel electrochemical activation effect induced morphology variation from massif-like Cu_xO to forest-like Cu₂O nanostructure and the excellent electrochemical performance as anode for Li-ion battery, *Electrochim. Acta* 96 (2013) 253–260.
- [38] J.C. Zhang, S.B. Ni, J. Tang, X.L. Yang, L.L. Zhang, The preparation of NiO/C-Ni composite as binder free anode for lithium ion batteries, *Mater. Lett.* 176 (2016) 21–24.
- [39] T. Brezesinski, J. Wang, S.H. Tolbert, B. Dunn, Ordered mesoporous α-MoO₃ with iso-oriented nanocrystalline walls for thin-film pseudocapacitors, *Nat. Mater.* 9 (2010) 146–151.

- [40] V. Augustyn, J. Come, M.A. Lowe, J.W. Kim, P.L. Taberna, S.H. Tolbert, H.D. Abruna, P. Simon, B. Dunn, High-rate electrochemical energy storage through Li⁺ intercalation pseudocapacitance, *Nat. Mater.* 12 (2013) 518–522.
- [41] J.C. Zhang, S.B. Ni, T. Kang, J. Tang, X.L. Yang, L.L. Zhang, Prominent electrochemical performance of a Li₃VO₄/C-Ni anode via hierarchically porous architecture design, *J. Mater. Chem. A* 4 (2016) 14101–14105.
- [42] Y. Shi, J.Z. Wang, S.L. Chou, D. Wexler, H.J. Li, K. Ozawa, H.K. Liu, Y.P. Wu, Hollow structured Li₃VO₄ wrapped with graphene nanosheets in situ prepared by a one-pot template-free method as an anode for lithium-ion batteries, *Nano Lett.* 13 (2013) 4715–4720.
- [43] J.L. Liu, J. Wang, C. Xu, H. Jiang, C. Li, L. Zhang, J. Lin, Z.X. Shen, Advanced energy storage devices: basic principles, analytical methods, and rational materials design, *Adv. Sci.* (2017), 1700322, 19p.